

Phase coherence and attractor geometry of chaotic electrochemical oscillators

Yong Zou, Reik V. Donner, Mahesh Wickramasinghe, István Z. Kiss, Michael Small et al.

Citation: *Chaos* **22**, 033130 (2012); doi: 10.1063/1.4747707

View online: <http://dx.doi.org/10.1063/1.4747707>

View Table of Contents: <http://chaos.aip.org/resource/1/CHAOEH/v22/i3>

Published by the [American Institute of Physics](http://www.aip.org).

Related Articles

Dissipative properties of systems composed of high-loss and lossless components

J. Math. Phys. **53**, 123508 (2012)

Disorder-induced dynamics in a pair of coupled heterogeneous phase oscillator networks

Chaos **22**, 043104 (2012)

Introduction to the Focus Issue: Chemo-Hydrodynamic Patterns and Instabilities

Chaos **22**, 037101 (2012)

Predicting the outcome of roulette

Chaos **22**, 033150 (2012)

Stability of discrete breathers in nonlinear Klein-Gordon type lattices with pure anharmonic couplings

J. Math. Phys. **53**, 102701 (2012)

Additional information on Chaos

Journal Homepage: <http://chaos.aip.org/>

Journal Information: http://chaos.aip.org/about/about_the_journal

Top downloads: http://chaos.aip.org/features/most_downloaded

Information for Authors: <http://chaos.aip.org/authors>

ADVERTISEMENT



AIP Advances

Submit Now

**Explore AIP's new
open-access journal**

- **Article-level metrics
now available**
- **Join the conversation!
Rate & comment on articles**

Phase coherence and attractor geometry of chaotic electrochemical oscillators

Yong Zou,^{1,2,3} Reik V. Donner,³ Mahesh Wickramasinghe,⁴ István Z. Kiss,⁴ Michael Small,^{2,5} and Jürgen Kurths^{3,6,7}

¹Department of Physics, East China Normal University, 200062 Shanghai, China

²Department of Electronic and Information Engineering, Hong Kong Polytechnic University, Hung Hom, Kowloon, Hong Kong

³Potsdam Institute for Climate Impact Research, Telegrafenberg A31, 14473 Potsdam, Germany

⁴Department of Chemistry, Saint Louis University, 3501 Laclede Ave., St. Louis, Missouri 63103, USA

⁵School of Mathematics and Statistics, University of Western Australia, Crawley, WA 6009, Australia

⁶Department of Physics, Humboldt University Berlin, Newtonstr. 15, 12489 Berlin, Germany

⁷Institute for Complex Systems and Mathematical Biology, University of Aberdeen, Aberdeen AB24 3UE, United Kingdom

(Received 19 March 2012; accepted 9 August 2012; published online 24 August 2012)

Chaotic attractors are known to often exhibit not only complex dynamics but also a complex geometry in phase space. In this work, we provide a detailed characterization of chaotic electrochemical oscillations obtained experimentally as well as numerically from a corresponding mathematical model. Power spectral density and recurrence time distributions reveal a considerable increase of dynamic complexity with increasing temperature of the system, resulting in a larger relative spread of the attractor in phase space. By allowing for feasible coordinate transformations, we demonstrate that the system, however, remains phase-coherent over the whole considered parameter range. This finding motivates a critical review of existing definitions of phase coherence that are exclusively based on dynamical characteristics and are thus potentially sensitive to projection effects in phase space. In contrast, referring to the attractor geometry, the gradual changes in some fundamental properties of the system commonly related to its phase coherence can be alternatively studied from a purely structural point of view. As a prospective example for a corresponding framework, recurrence network analysis widely avoids undesired projection effects that otherwise can lead to ambiguous results of some existing approaches to studying phase coherence. Our corresponding results demonstrate that since temperature increase induces more complex chaotic chemical reactions, the recurrence network properties describing attractor geometry also change gradually: the bimodality of the distribution of local clustering coefficients due to the attractor's band structure disappears, and the corresponding asymmetry of the distribution as well as the average path length increase. © 2012 American Institute of Physics. [<http://dx.doi.org/10.1063/1.4747707>]

Chaotic oscillations are a wide-spread phenomenon that can be observed in many natural and technological systems.^{1,2} The complex dynamics of such systems is characterized by an exponential divergence of initially close trajectories as time proceeds.^{3–5} As a consequence, long-term predictions of the amplitudes and phases are not possible. The degree of dynamical complexity of chaotic oscillators can be measured in terms of various quantities from nonlinear time series analysis and complex systems theory,^{6,7} such as Lyapunov exponents, fractal dimensions, or entropies and related concepts from information theory. In addition to these widely applicable concepts, the phase coherence of chaotic oscillations has been recently recognized as an important complementary aspect. While this feature has been previously considered based on its manifestation in various nonlinear dynamical characteristics, in this work, we provide arguments that phase coherence should rather be viewed as a structural property of chaotic attractors in phase space. For a well-studied example of electrochemical chaos, we demonstrate that complex dynamics emerges without qualitative changes in attractor geometry related to a loss of phase

coherence. This calls for the development of alternative geometric criteria for the presence of phase coherence replacing the present purely dynamics-based perspective.

I. INTRODUCTION

In the last about 15 years, there has been a rising interest in phase synchronization processes between coupled oscillatory systems.^{8,9} Studies of such processes are traditionally based on the consideration of a well-defined quantity $\phi(t)$ describing the observed phase dynamics of each individual system. The existence of such a meaningful phase variable is closely related to the notion of *phase coherence* as a key property of chaotic oscillators. Specifically, the standard analytical signal approach⁹ to define a phase from a univariate observational time series, which is most often used in the literature, explicitly requires phase-coherent oscillations in the sense of a well-defined center of oscillations in a two-dimensional projection of the observed system.^{10–12} Although there are alternative approaches allowing to numerically

characterize phase synchronization also for systems that do not meet this requirement,^{10,11,13} there is a persistent interest in distinguishing whether or not a chaotic system under study is phase coherent.

While the term phase coherence is usually well-defined in connection with the analysis of wave-like phenomena in optics and acoustics, its actual meaning in a dynamical systems context has remained somewhat ambiguous so far. Here, the main interest in phase coherence is associated with the goal of understanding and quantitatively characterizing different types of complex chaotic dynamics. However, since it is known that the appearance of attractors can strongly depend on the variable used for their reconstruction,¹⁴ the presence of phase coherence in the aforementioned sense can also depend on the particularly chosen observation function and does not necessarily relate to certain structural properties of a chaotic attractor. This work is intended to contribute to a more rigorous discussion of the interrelationships between phase coherence and attractor geometry, which have been widely overlooked so far by considering phase coherence exclusively in the context of dynamics.

As a particular example, we analyze the dynamic properties as well as structural features of the reconstructed attractors associated with chaotic electrochemical oscillations obtained from both experiments and a corresponding mathematical model. It has already been demonstrated¹⁵ that the dynamical complexity of the considered system strongly changes as one fundamental control parameter (temperature) is varied. Here, we investigate the associated variations in both dynamic complexity and structural organization of the system in its phase space. By careful analysis, we delineate whether the previously associated changes in phase coherence could be considered as a result of gradual changes of the attractor structure, or there exists a major (discontinuous) qualitative change of the attractor geometry in phase space that corresponds to a deterioration of phase coherence.

This paper is organized as follows: In Sec. II, we review existing concepts of phase coherence and show that the resulting properties strongly depend on the selected observable of the system and can provide misleading results due to projective effects during attractor reconstruction. This motivates discussing a more general structural point of view on phase coherence, which is exclusively associated with the geometric structure of a chaotic attractor in phase space and does not directly relate to the associated dynamics. As an example, we discuss implications for the identification of phase coherence in chaotic electrochemical oscillations in Sec. III. A detailed characterization of the corresponding structural attractor properties is presented in Sec. IV by considering concepts from complex network theory. Finally, the main conclusions of this work are summarized in Sec. V.

II. DYNAMIC VS. GEOMETRIC VIEWS ON PHASE COHERENCE

In electromagnetism, optics, or acoustics, the term phase coherence is commonly used for describing (i) the quality of a wave to display a well-defined phase relationship in different regions of its domain of definition, (ii) the existence of

significant statistical correlations between the phases of two or more waves, or (iii) the presence of a state in which two signals maintain a fixed phase relationship with each other or with a third signal. We emphasize that when identifying the aforementioned waves with general oscillatory signals obtained from complex systems (as we will be dealing with in this work), aspects (ii) and (iii) relate to the concept of phase synchronization of coupled oscillatory systems.^{8,9}

A. Phase coherence and power spectrum

In a dynamical systems context, the term “phase coherence” has been originally coined by Farmer *et al.*¹⁶ for describing the qualitatively different appearances of power spectra of chaotic systems associated with their respective mixing behavior. Specifically, a chaotic attractor is considered phase-coherent if its power spectral density (PSD) is a superposition of δ -functions and a broad background typical for general chaotic systems. The corresponding phenomenon has been elsewhere referred to as *nonmixing chaos*^{17,18} or *noisy periodicity*.¹⁹

According to the latter notion of phase-coherent chaos, it has been conjectured that strange attractors arising from sequences of period-doubling bifurcations are phase-coherent.^{19–21} Successful applications include studies of strange attractors in coupled reaction-diffusion cells,²² the frequency entrainment of chaotic oscillators subject to periodic forcing,²³ and transient chaotic systems with a tunable degree of phase coherence.²⁴

The characteristic properties of the system’s PSD relevant for the identification of phase coherence are not appropriately reflected by traditional measures of nonlinear dynamics such as the Lyapunov exponent or Kolmogorov entropy.¹⁶ In turn, there are several statistical properties quantifying the degree of heterogeneity of the PSD (and, hence, the “degree of phase coherence”) that can be used for this purpose, including the production of spectral entropy²⁵ or degrees of freedom^{16,26–28} and conceptually related measures.

B. Definition of phase variables

The rising interest in the numerical analysis of phase synchronization phenomena has led to a conceptually different notion of phase coherence associated with the presence of a well-defined phase variable $\phi(t)$. The existence of such a phase variable ultimately depends on the structural organization of the studied system in its phase space. Specifically, for an oscillatory signal $x(t)$ (no matter whether regular or chaotic), we require that the associated phase variable $\phi(t)$ increases monotonously with time in a phase-coherent regime. In this spirit, one can use a simple measure for the monotonicity of $\phi(t)$, the so-called *coherence index*²⁹

$$CI = \lim_{T \rightarrow \infty} \frac{1}{T} \int_0^{\infty} \Theta(-\dot{\phi}(t)) dt, \quad (1)$$

for quantitatively characterizing the degree of possible non-phase-coherence associated with a particular $\phi(t)$. In the latter definition, $\Theta(\cdot)$ denotes the Heaviside function.

There is a variety of possibilities to define a phase variable $\phi(t)$.^{9,30} In general, we consider it as being derived from a feasible low-dimensional projection $(\xi_1(t), \xi_2(t))$ of the system under study as

$$\phi(t) = \arctan \frac{\xi_2(t)}{\xi_1(t)}. \quad (2)$$

For a scalar observable $x(t)$, a general and widely applied approach is to define a phase by means of an analytical signal approach (i.e., the complex continuation of $x(t)$) by identifying $\xi_1(t)$ with $x(t)$ and $\xi_2(t)$ with its Hilbert transform

$$H(x(t)) = \frac{1}{\pi} \mathcal{P.V.} \int_{-\infty}^{\infty} \frac{x(s)}{t-s} ds, \quad (3)$$

where $\mathcal{P.V.}$ denotes Cauchy's principal value of the integral. The thus defined variable $\phi(t)$ increases monotonously with time if the oscillatory dynamics has a common center of all rotations at the origin of the complex $(x, H(x))$ plane. If this condition is not fulfilled, several authors proposed using an alternative phase definition based on the local curvature properties of the analytical signal^{10–12} by setting $\xi_1(t) = \dot{x}(t)$ and $\xi_2(t) = \dot{H}(x(t))$. The latter approach has demonstrated its potentials for providing a proper phase definition for certain non-phase-coherent chaotic oscillators such as the funnel regime of the Rössler system.³¹ In turn, it is less efficient in case of noisy oscillations where other, more sophisticated approaches are needed for characterizing phase synchronization and phase coherence.^{13,32}

A widely used method for characterizing the presence or absence of phase coherence of chaotic oscillations is based on concepts from statistical physics. Specifically, under certain assumptions, the dynamics of the phase variable $\phi(t)$ can be approximated by a random walk with a fixed drift determined by the mean frequency ω of oscillations. In this case, the second-order structure function

$$F_2(s) = \langle [\phi(t+s) - \phi(t) - 2\pi\omega s]^2 \rangle \simeq D_\phi s + \text{const} \quad (4)$$

of the detrended phase allows estimating the phase diffusion coefficient D_ϕ of the system under study by means of linear regression.^{9,15,33–35} In the case of phase-coherent oscillations, this quantity should approach 0 in the asymptotic limit, whereas it is expected to be strictly positive for non-phase-coherent (or, for short, noncoherent) oscillations. We note, however, that the proper numerical estimation of D_ϕ can be a challenging task. Alternatively, one can use the coherence factor^{33,36,37}

$$CF = \langle T \rangle / \sigma_T \quad (5)$$

based on the mean return time $\langle T \rangle$ of the trajectory with respect to a certain Poincaré surface in the (ξ_1, ξ_2) plane and the associated standard deviation σ_T . The basic challenge of the latter approach is the appropriate definition of the Poincaré section to be considered.

We emphasize that the notion of phase coherence based on some specific phase variable $\phi(t)$ generally characterizes only a property associated with a particular two-dimensional

projection of the system (e.g., one coordinate $x(t)$ and its Hilbert transform, or two selected coordinates), but not necessarily the chaotic attractor as a whole. Under rather general conditions, this attractor can be topologically equivalently reconstructed from a single coordinate $x(t)$ by means of time-delay embedding.^{38,39} (Note that the definition of the Hilbert phase does *not* incorporate this technique). In this spirit, chaotic oscillators are always characterized by different degrees of freedom, i.e., different dynamically relevant variables. Depending on the choice of observable, the reconstructed attractor may exhibit different structural properties.¹⁴ Therefore, using different coordinates can also lead to phase variables with different monotonicity properties.

We give a simple example: If a given scalar signal $x(t)$ is *not* properly centered around 0 (i.e., we do *not* have that all local minima are located at $x < 0$ and all local maxima at $x > 0$), the Hilbert transform approach leads to a phase variable with a non-monotonous behavior. However, if there is some $x_0 \neq 0$ such that all local maxima have $x > x_0$, and all local minima $x < x_0$ (i.e., all oscillations of the system are centered at x_0), a simple translation $x' = x - x_0$ provides a new coordinate which has the desired property of a monotonous Hilbert phase. More general, there can be transformations of the system's coordinates that leave the dynamics invariant, but lead to a coherent Hilbert phase. In this respect, notions of phase coherence relating to either the consideration of power spectra or specific phase variables are always based on certain projections of the system rather than the overall structural organization of the attractor.

C. Phase coherence as a structural attractor property

Besides the aforementioned conceptual limitations, both previous notions of phase coherence suffer from the additional problem that there is no simple statistics that clearly distinguishes between phase coherent and non-phase-coherent chaotic oscillations. This statement especially applies to the characterization of phase coherence based on the power spectrum, particularly regarding the variance of the underlying estimator (e.g., the periodogram) and the possible presence of significant observational noise in case of experimental data. In turn, for the Hilbert phase and related approaches, the correct estimation of measures such as the phase diffusion coefficient or coherence factor—particularly from experimental time series—can also be a challenging task.²⁹ This suggests that in the case of experimental applications, one should compare various definitions of phase coherence and carefully discuss which measure is the most appropriate in practice.

Following the previous considerations, we propose considering the *structural phase coherence* of chaotic oscillators as the existence of a coordinate transformation that allows deriving a monotonously increasing phase variable (e.g., by means of the standard Hilbert transform method). That is, there exists a two-dimensional (linear or nonlinear) projection of the attractor under which it takes an approximately toroidal shape, i.e., the attractor has the shape of a smeared limit cycle. Note that this notion of structural phase coherence is more general than the (projective) phase coherence

relating to the dynamical attractor properties captured in its PSD or phase diffusion properties.

D. Examples

As already mentioned above, in many situations, a linear transformation (i.e., translation or rotation) of the (reconstructed) attractor leads to a coordinate with a coherent Hilbert phase. However, this is not always possible.

A prominent example for a chaotic system with truly non-coherent dynamics is the funnel attractor of the Rössler system. Here, the chaotic attractor undergoes fundamental structural changes accompanying a transition between phase-coherent and noncoherent dynamics due to a collision of the growing chaotic attractor with some homoclinic orbit of the system, which is reflected by a sharp transition in the associated dynamical as well as geometric properties.^{13,29} As a result, there is no simple linear transformation (or projection) of the system's coordinates that leads to rotations with a well-defined center. We conjecture that such an abrupt change is typical for a chaotic system with missing structural phase coherence.

As an example for a chaotic system whose oscillations are noncoherent with respect to some of the original coordinates, but phase-coherent after a sophisticated nonlinear coordinate transformation, consider the Lorenz system⁴⁰

$$\begin{aligned}\dot{x} &= 10(y - x), \\ \dot{y} &= x(28 - z) - y, \\ \dot{z} &= xy - 8/3z\end{aligned}\quad (6)$$

at the canonical parameter values (see Fig. 1(a)). Letellier and Aguirre¹⁴ argued that due to the symmetry of the system (6), time-delay embedding of x - and y -coordinates leads to double-scroll attractors, whereas using the z -coordinate naturally leads to a phase-coherent single-scroll attractor. By a coordinate transform $(x', y', z') = (x^2 - y^2, 2xy, z)$, one obtains the proto-Lorenz equations,^{14,41,42} for which the projection into the (y', z') plane obeys a well-defined center of rotations. Alternatively, introducing a new coordinate $u = \sqrt{x^2 + y^2}$ (Ref. 9) (i.e., the Euclidean norm in the (x, y) plane) also maps the two scrolls of the chaotic attractor onto each other in the (u, z) plane (Fig. 1(b)). In this spirit, the Lorenz system (with the canonical parameters) is considered structurally phase-coherent. Even more, unlike the original x -coordinate, consideration of the transformed variable u also reveals different other features typical for the established notions of phase coherence, such as a peak in the PSD indicating the presence of a natural frequency (Fig. 1(d)), and a low variance of the linearly detrended Hilbert phase indicating a low phase diffusion coefficient (Fig. 1(h)).

III. EXPERIMENTAL TIME SERIES

A. Experimental setup

As an example of real-world chaotic oscillations, we consider data obtained from chemical experiments with Ni electrodisolution in 4.5 mol/l sulfuric acid. At eight temperatures in the range of 2 °C–30 °C, time series of the electric current have been recorded at conditions that produce

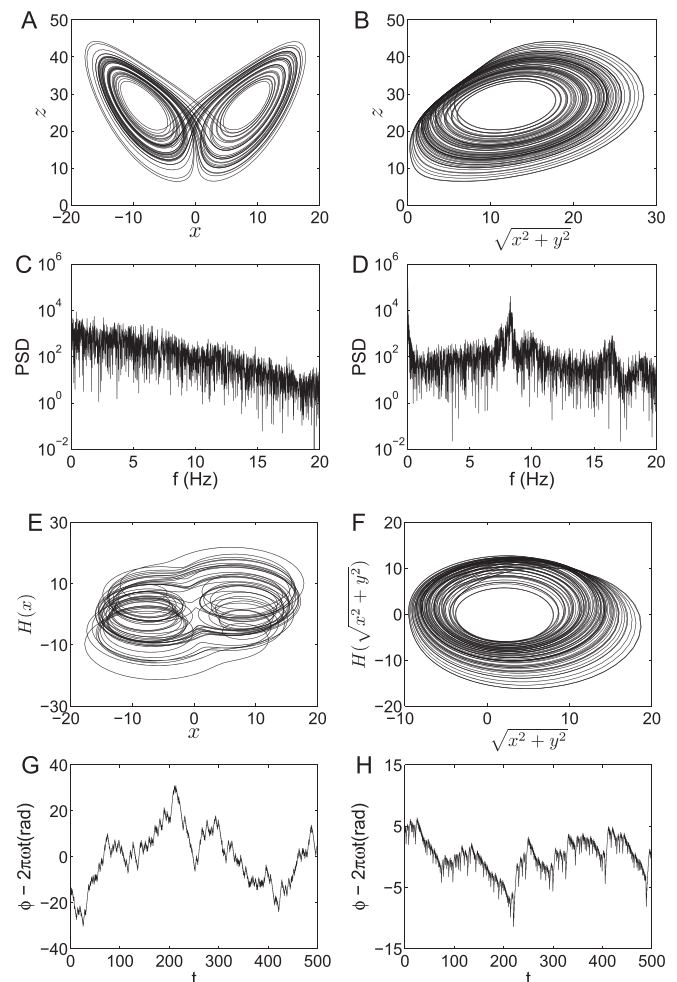


FIG. 1. Effect of different projections of the Lorenz system (6) based on its x - (left panels) and u -variable (right panels): (a) (x, z) - and (b) (u, z) -projections, ((c) and (d)) periodograms as estimates of the PSD for the (c) x - and (d) u -coordinates, ((e) and (f)) Hilbert transforms (after correcting for the mean values), and ((g) and (h)) resulting time evolution of the detrended Hilbert phases.

chaotic oscillations. A typical data file consisted of about 1250 oscillations with 185 data points per cycle. Further details on the experimental conditions have been given in a previous publication.¹⁵

B. Preprocessing of the data

From the measured scalar time series, we reconstruct the underlying chaotic attractor in phase space by means of time-delay embedding.^{38,39} Specifically, we select an embedding dimension $m = 3$ and determine appropriate values for the embedding delay τ by considering the decorrelation time (i.e., the time lag after which the autocorrelation function of the signal has fallen below $1/e$). We emphasize that our particular choice of m presents a trade-off between properly representing the underlying dynamics (which could eventually take place in a higher-dimensional phase space) and the possibility of visualizing the results of our analysis in the reconstructed phase space. However, independent analyses with higher values of m yield results (not shown) which are qualitatively similar to those described in the following, indicating the actual presence of low-dimensional chaos.

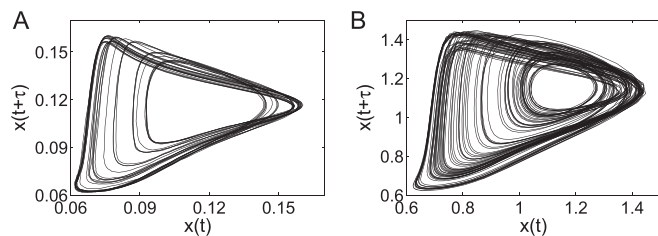


FIG. 2. Projections of the reconstructed attractors for (a) case I and (b) case II.

In order to avoid potential transient effects in the beginning of all experimental runs, the first 1000 data points have been removed from all records. Moreover, since the experimental time series have been sampled at very high rates, all records have been downsampled by a factor of five.

C. Dynamical characteristics: Two examples

Before systematically discussing the influence of changing experimental conditions on dynamics and attractor geometry associated with the property of phase coherence of the observed chaotic oscillations in some detail, we first describe the extreme cases observed in this study corresponding to low (case I, 2 °C) and high temperatures (case II, 30 °C), respectively. In order to obtain a feasible visualization of the respective attractors, we have considered the following embedding delays: $\tau_1 = 75$ (375 ms) and $\tau_2 = 30$ (30 ms, note the different data acquisition rate in both experiments). Note again that the results of our analyses described in the following do not differ markedly if these embedding parameters are altered within acceptable limits.

In order to visually highlight the different appearances of the chaotic electrochemical oscillations observed in this study, Fig. 2 displays the corresponding attractor structure in a two-dimensional projection of the reconstructed phase space for the considered experimental settings. In both scenarios, we find a distinct center of oscillations, which however becomes narrower (i.e., less well-expressed) in the high-temperature case II. Although the reported phase diffusion coefficient of the chaotic process is enhanced by a factor of 18,¹⁵ the qualitative similarity of the general appearance of the attractors in the reconstructed phase space indicates that the experimental conditions do not exhibit a transition to a structurally noncoherent chaotic attractor. In contrast, the dynamic complexity (characterized by concepts such as Lyapunov exponent or information dimension) rises considerably with increasing temperature.¹⁵ We further illustrate these findings by considering three additional characteristics of the chaotic dynamics: the PSD, recurrence time distributions, and 2nd-order Rényi entropy.

The PSD (Figs. 3(a) and 3(b)) reveals a broad continuum of frequencies contributing to the observed dynamics, which is typical for chaotic oscillations. In the low-temperature case (Fig. 3(a)), we find a distinct set of frequencies with enhanced spectral power (note the logarithmic axis) corresponding to the dominating instantaneous frequencies of the chaotic oscillator. In contrast, such marked spectral peaks are less obvious in the high-temperature case (Fig. 3(b)).

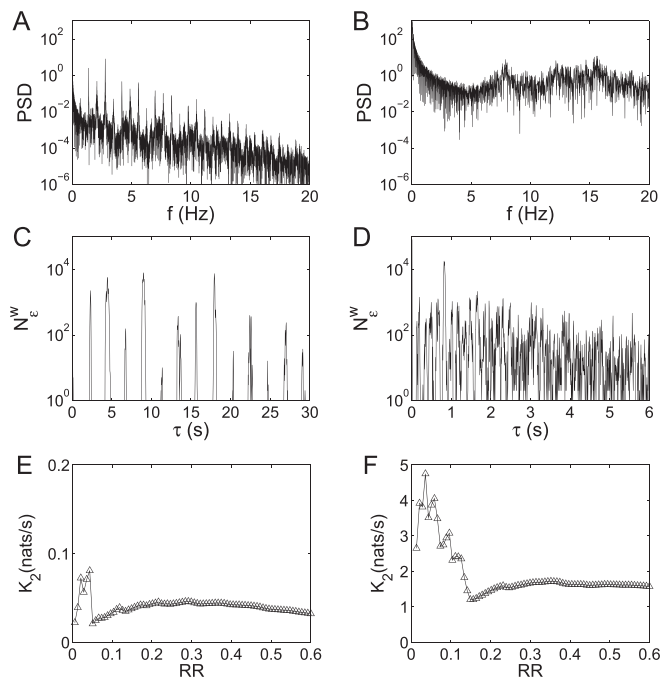


FIG. 3. ((a) and (b)) Periodogram as an estimator of the PSD, ((c) and (d)) recurrence time distributions $p(\tau)$ (zooms for short times and low frequencies), and ((e) and (f)) estimated 2nd-order Rényi entropy K_2 for different values of RR for the chaotic electrochemical oscillations in ((a), (c), (e)) low-temperature case I and ((b), (d), (f)) high-temperature case II.

Beyond the PSD describing only linear statistical properties of the observed time series, we further utilize two statistical characteristics based on the evolution of the systems' recurrence properties in phase space. It is known that recurrences capture important aspects of the dynamics of the associated complex system,^{43,44} particularly including information on its nonlinear characteristics. For convenience, their temporal pattern is encoded in *recurrence plots* (RPs) associated with a single recorded time series or trajectory.^{45,46} Here, a RP is the visual representation of the *recurrence matrix* of binary neighborhood relationships between all pairs of observed state vectors $\vec{x}_i = \vec{x}(t_i)$, $i = 1, \dots, N$ (which can combine either the individual components of a multivariate time series, or the dynamically relevant modes reconstructed from a univariate signal by means of time-delay embedding), defined as

$$R_{i,j}(\varepsilon) = \Theta(\varepsilon - \|\vec{x}_i - \vec{x}_j\|), \quad (7)$$

where $\Theta(\cdot)$ is again the Heaviside function, $\|\cdot\|$ is a norm (e.g., Euclidean, Manhattan, or maximum norm) in the considered phase space, and ε is a prescribed maximum distance for defining the neighborhood of individual state vectors. The appearances of RPs distinctively differ between qualitatively different types of dynamic behavior.⁴⁶

For the quantitative assessment of RPs, several distinct approaches can be distinguished: First, RPs allow directly estimating the values of certain dynamical invariants such as the correlation dimension D_2 and the 2nd-order Rényi entropy K_2 of the system under study.^{47–49} Second, a variety of additional complexity measures characterizing different

aspects of the dynamical behavior of the system (such as the degrees of determinism and laminarity) is provided by the so-called recurrence quantification analysis (RQA).^{50–53} Third, recurrence time statistics (i.e., the analysis of the distribution $p(\tau)$ of time differences between the system leaving and re-entering the neighborhood of a specific state vector) allows distinguishing different types of dynamic behavior.^{54–56} Finally, ε -recurrence networks (RNs) provide a graph-theoretical framework for quantifying various aspects of the underlying attractor's geometry.^{29,57–67}

In the following, we will use $p(\tau)$ and K_2 for further characterizing the dynamical complexity of the observed electrochemical oscillations. For this purpose, we will restrict our attention to the first $N = 10\,000$ points of the embedded time series in order to keep the computational efforts at an acceptable level. The corresponding recurrence rate $RR(\varepsilon) = \sum_{i \neq j} R_{i,j}(\varepsilon) / (N(N-1))$ will be kept fixed at $RR = 0.03$ (i.e., the value of ε is adaptively chosen accordingly) for the recurrence time statistics, but considered variable for the estimation of K_2 .^{46,47}

In comparison with the PSD, the recurrence time distributions $p(\tau)$ (Figs. 3(c) and 3(d)) reveal even stronger differences between low- and high-temperature regimes: At low temperatures, the distribution is characterized by regularly spaced peaks at multiples of a basic recurrence period (Fig. 3(c)), whereas it appears much more irregular in the high-temperature regime with a variety of incommensurable frequencies contributing to the dynamics (Fig. 3(d)). This qualitative behavior indicates marked differences in the distribution of periods of unstable periodic orbits (UPOs) densely embedded in the chaotic attractors present in both regimes. Specifically, the two recurrence time distributions closely resemble those obtained for the standard (phase-coherent) Rössler system and the associated (non-phase-coherent) funnel attractor.²⁹

Finally, we study the 2nd-order Rényi entropy K_2 computed from the RPs for different values of RR (see Ref. 46, for details on the used estimator). We clearly observe that in the low-temperature regime, the recorded dynamics of the electrochemical oscillations is by far less complex (lower K_2) than at higher temperatures (plateau values in Figs. 3(e) and 3(f) for sufficiently large RR). This finding is consistent with the less complex pattern of the recurrence time distribution as well as the more pronounced spectral peaks at lower temperatures.

D. Phase definition and projective effects on phase coherence analysis

As already discussed in great detail, a meaningful study of phase coherence properties first requires a suitable selection of a specific observable in order to be able to define a proper phase variable. In the following, we will demonstrate for the two example cases of chaotic electrochemical oscillations discussed above how this choice can result in inappropriate conclusions on the presence of phase coherence. For simplicity, we will restrict our attention here to linear (affine) coordinate transformations, i.e., $\vec{x}' = \mathbf{A}\vec{x} + \vec{x}_0$, particularly translations and rotations, of the original observable x .

In a previous paper,¹⁵ estimates of D_ϕ based on the curvature method (i.e., derivatives of $x(t)$ and its Hilbert trans-

form) have been used to conclude that only in the low-temperature case I, phase-coherent oscillations are unambiguously present, whereas the dynamical characteristics of the high-temperature case II resemble those of noncoherent oscillations (cf., Sec. III C). However, even in the latter regime, phase-coherent oscillations could be present when considering our more general perspective. In order to clarify the extent by which the observed changes in the dynamical characteristics actually originate from changing phase coherence properties, we will next examine the geometric structure of the strange attractor reconstructed from the recorded chaotic oscillations $x(t)$ (see Fig. 4) in more detail.

Following a standard procedure of phase synchronization analysis, we start by removing the mean of the original time series as

$$y(t) = x(t) - \langle x(t) \rangle \quad (8)$$

with $\langle x(t) \rangle \approx 1.18$ in the high-temperature regime (cf. Fig. 2(b)). Next, we reconstruct the chaotic attractor by time-delay embedding with the embedding parameters described above. By means of visual inspection of a two-dimensional projection of the thus embedded series (Fig. 4(a)), we identify well-expressed rotations which, however, do not always contain the origin of the reconstructed coordinate system (cf. the corresponding marker). Specifically, the observed chaotic oscillations sometimes have local minima at values $y > 0$ (Fig. 4(c)), so that the computation of the Hilbert transform reveals rotations with a marked center in the $(y, H(y))$ plane (Fig. 4(e)), which do not always include the origin. As a consequence, the Hilbert phase $\phi(t)$ based on these coordinates does not monotonously increase in time, and we observe a relatively large variance of the detrended phase (Fig. 4(g)) giving rise to non-zero values of the phase diffusion coefficient.

Relating to our conceptual idea of structural phase coherence, the offset of the well-defined center of rotations in the two-dimensional projection $(y(t), y(t + \tau))$ calls for a proper redefinition of the corresponding coordinates by means of a linear transformation of the reconstructed attractor. Figure 4(b) displays the coherence index CI for the Hilbert phase of the rotated coordinate

$$y_{opt}(t) = \cos\psi y(t) + \sin\psi y(t + \tau), \quad (9)$$

as a function of the rotation angle ψ in the $(y(t), y(t + \tau))$ plane. For certain values of ψ , the coherence index becomes zero, indicating that the Hilbert phase for the thus obtained new variable (Fig. 4(d)) is a monotonous function of time in the respective range of ψ . (A similar result can also be found after a suitable translation of y .) Hence, the oscillations in the $(y_{opt}(t), H(y_{opt}(t)))$ plane have a well-defined center, and all rotations include the origin of the transformed coordinate system (Fig. 4(f)). As a consequence, the resulting detrended phase has a variance which is by about one order of magnitude smaller than that originally computed for $y(t)$ (Fig. 4(h)) (in fact, the phase dynamics associated with the rotated coordinates much more resembles a diffusion process than that obtained from the original coordinate). However, from our conceptual perspective, the dynamics is structurally

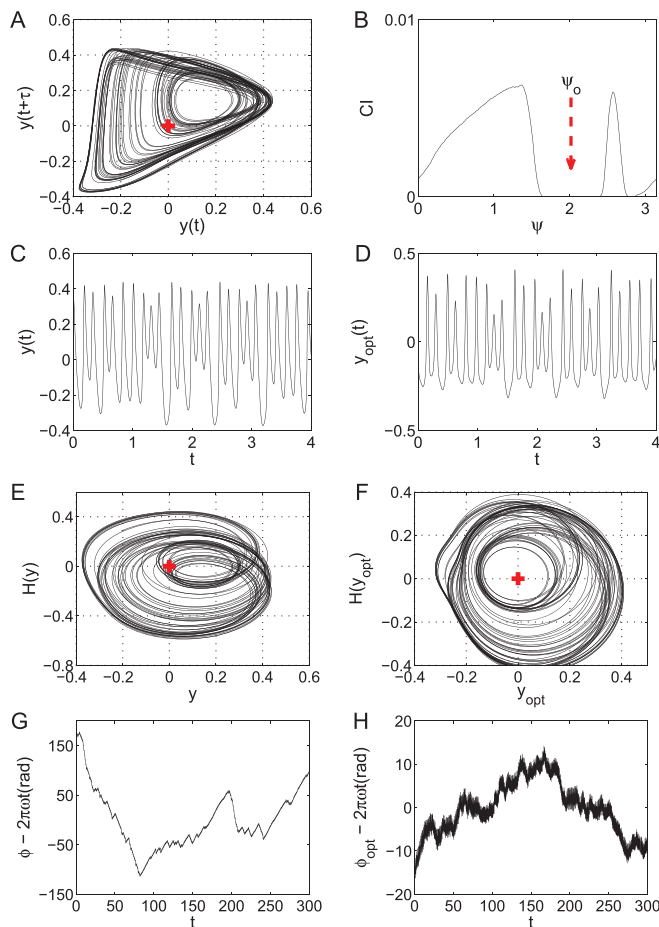


FIG. 4. Phase coherence analysis in the high-temperature case II (cf. Fig. 2(b)): (a) Parts of the trajectory projected onto the $(y(t), y(t + \tau))$ plane of the reconstructed phase space. (b) Variation of the coherence index CI (Eq. (1)) in dependence on the rotation angle ψ in the considered plane. (c) and (d) Parts of the trajectory of the original (y) and optimized (y_{opt}) coordinate. The latter one has been obtained by rotating the $(y(t), y(t + \tau))$ plane about an angle of $\psi_0 = 2$. (e) and (f) Reconstructed oscillations in the $(y, H(y))$ plane for the original and rotated coordinate. (g) and (h) Dynamics of the linearly detrended phase obtained from the original and reconstructed coordinate.

phase-coherent, even though the phase diffusion coefficient estimated from the finite time series does still take non-zero values due to the high dynamic complexity (cf. the corresponding values of K_2 in Sec. III C). To put it differently: given Fig. 4(h) alone, it would remain ambiguous whether or not the studied process is phase-coherent. In turn, Fig. 4(f) clearly displays the qualitative picture one typically has in mind when speaking of phase-coherent chaotic oscillations.

The above example demonstrates the importance of projection effects on the outcomes of phase coherence analysis. Following our considerations, an improper choice of observation function could even destroy the signature of the clearly phase coherent low-temperature regime (case I) in measures based on the Hilbert transform.

E. Phase coherence of experimental electrochemical oscillations

In Ref. 15, it has already been demonstrated that the chaotic electrochemical oscillations under study undergo gradual

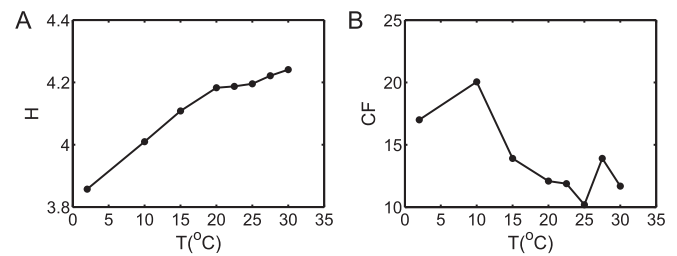


FIG. 5. (a) Shannon entropy H of Poincaré intersection points through the surface $y_{opt} = 0$, $\dot{y}_{opt} < 0$ (estimated using a histogram of 80 equi-sized bins), for experimental runs at different temperatures. (b) Coherence factor CF as a measure of phase coherence.

changes towards a higher degree of complexity as the temperature increases. In the spirit of our previous considerations, we now systematically examine how this is reflected in the phase coherence properties of the underlying attractor. For this purpose, we choose the reference variable $y_{opt}(t)$ similar to the way described above for the high-temperature regime. Specifically, in all considered experimental runs, a simple translation of the observable allows defining a feasible coordinate for which the two-dimensional projection of the reconstructed attractor displays a well-defined center of rotations around the origin. (Additional rotations are not required here.)

Figure 5(a) shows that the increasing dynamic complexity of the system is accompanied by an increasing variety of points in some Poincaré section of the system. At the same time, the associated coherence factor CF decreases (Fig. 5(b)) due to the increasing variation of associated return times. However, being able to properly define the Poincaré surface according to our coordinate transformation, we can conclude that in all considered experimental settings, the system is phase coherent (i.e., $CF \gg 1$). These observations indicate an increasing spread of unstable periodic orbits embedded in the chaotic attractor and, hence, a larger “dispersion” of the attractor itself, which is consistent with the qualitative appearance in Fig. 2 and the more complex dynamics previously reported. Next, we will further quantitatively characterize the corresponding subtle variations of the structural properties of the attractor.

IV. STRUCTURAL ATTRACTOR CHARACTERIZATION

As a further extension of the previous discussions on changes of the dynamical complexity with increasing temperature, in the following we will provide complementary results relating to the structural properties of the attractor in phase space. For this purpose, we utilize the concept of RNs.^{57,58,61} For computational reasons, we will again restrict ourselves to networks constructed from $N = 10\,000$ state vectors in the considered reconstructed phase space and a fixed recurrence rate of $RR = 0.03$. Specifically, for the experimental data, we can consider ensembles of randomly drawn state vectors, since RN analysis only requires a reasonable spatial sampling of the attractor, but no time information.^{58,61}

A. Recurrence network analysis

In order to construct a RN from an observed time series of a dynamical system, we remove the main diagonal of the

recurrence matrix R_{ij} to obtain the adjacency matrix A_{ij} of an undirected complex network, i.e.,

$$A_{ij}(\varepsilon) = R_{ij}(\varepsilon) - \delta_{ij}, \quad (10)$$

where δ_{ij} is the Kronecker delta. The vertices of the RN can be identified with state vectors on the sampled trajectory; the connectivity is established according to the mutual proximity of these vectors in phase space. The considered definition provides a generic way for studying geometric properties of chaotic attractors by means of complex network methods.^{29,58,64} In turn, the properties of RNs do *not* capture the dynamics on the attractor.

It is important to point out that a RN is an approximation of an underlying continuous graph with uncountably many vertices and edges associated to the attractor in the corresponding phase space.⁶⁵ Specifically, RNs are random geometric graphs, the properties of which are fully determined by the system's continuous invariant density $p(\vec{x})$. Hence, the RN characteristics studied in the following are *discrete* estimators of some (continuous) attractor properties. Therefore, $p(\vec{x})$ needs to be properly sampled in space for constructing the RN (i.e., the sampled state vectors must largely cover the attractor⁶³). Note that this requirement is distinctively different from the typical sampling considerations in the time domain, although the resulting effects might be the same for a chosen trajectory of an ergodic system. As a result, the computed global and local properties of the RN are reasonable estimates of the associated attractor properties reflecting spatial scales $\geq \varepsilon$. This is, the smaller ε , the higher the spatial resolution, but the more sampled state vectors need to be taken into account for obtaining proper estimates of the RN characteristics. Since we consider here randomly sampled state vectors from very long trajectories including many oscillations of the observed system, we argue that the above considerations are very well met in our case. Specifically, we can practically exclude the presence of sojourn points representing spatial signatures of trivial temporal auto-correlations (i.e., subsequent observations) in the RN that could eventually lead to some bias in the resulting quantitative network properties. As a consequence, our sampling strategy yields qualitatively and quantitatively robust results.

The interpretations of global as well as local RN properties in terms of attractor geometry, as well as their dependence on network size,⁶⁵ embedding,⁶⁰ sampling,^{61,68} and other factors have already been studied elsewhere. In this work, we will use a complementary set of RN characteristics^{69–71} that have already demonstrated their capabilities to distinguish qualitatively different types of dynamics based on structural attractor properties^{29,57,63}

1. The *local* clustering coefficient C_v quantifies the relative amount of closed triangles centered at a given vertex v (i.e., at the associated point \vec{x}_v in phase space).
2. Betweenness centrality b_v quantifies the fraction of shortest paths in the network that contain a given vertex v .⁷² In a RN, vertices with high b_v correspond to regions of phase space with low density of the attractor that are located between higher density regions, so that b_v yields information about the local fragmentation of the attractor.^{58,60} For

convenience, we will consider $\log b_v$ as a characteristic measure in the following.

3. The *global* (Watts-Strogatz) clustering coefficient C (Ref. 73) gives the arithmetic mean of the local clustering coefficient C_v taken over all vertices v .
4. Network transitivity \mathcal{T} (Refs. 74 and 75) globally characterizes the linkage relationships among triples of vertices in the entire network (i.e., the probability of a third edge within a set of three vertices given that the two other edges are already known to exist). Sometimes, this measure is referred to as the (Barrat-Weigt) clustering coefficient, since it captures a similar property as C .
5. The average path length \mathcal{L} gives the average shortest graph distance between all possible pairs of vertices.
6. The assortativity coefficient \mathcal{R} (Ref. 76) measures the correlations between the numbers of connections at both ends of the same edge taken over the whole network.

We emphasize that both local RN properties (C_v and $\log b_v$) are sensitive to the presence of unstable periodic orbits (especially UPOs of lower periods),⁶⁰ which form the geometric backbone of chaotic attractors. Since the spatial distribution and repulsivity of the individual UPOs are responsible for the emergence of distinct peaks in the PSD associated with a chaotic oscillator, they play an important role for the presence or absence of phase coherence in both the (statistical) dynamical and structural senses.

B. Example cases

In order to gain first insights into structural differences between the chaotic attractors at high and low temperatures, we reconsider the two regimes already discussed in Sec. III C with respect to their dynamical characteristics. Figure 6 shows the spatial patterns of the local RN measures C_v and $\log b_v$. We note that the overall patterns are qualitatively similar for both situations, although the underlying attractor experiences a successive deformation when increasing the temperature as the fundamental control parameter of the system. This deformation is reflected in the fine-structure of the corresponding spatial distribution of RN vertex characteristics.

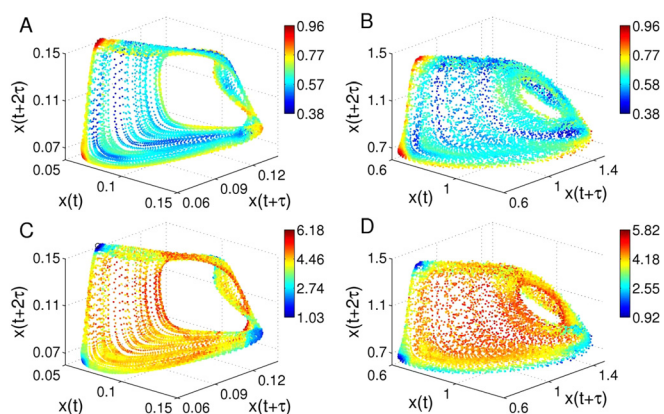


FIG. 6. Color-coded representations of the local RN properties ((a) and (b)) C_v and ((c) and (d)) $\log b_v$ for the experimental data of electrochemical oscillations in ((a) and (c)) low-temperature (case I) and ((b) and (d)) high-temperature regime (case II).

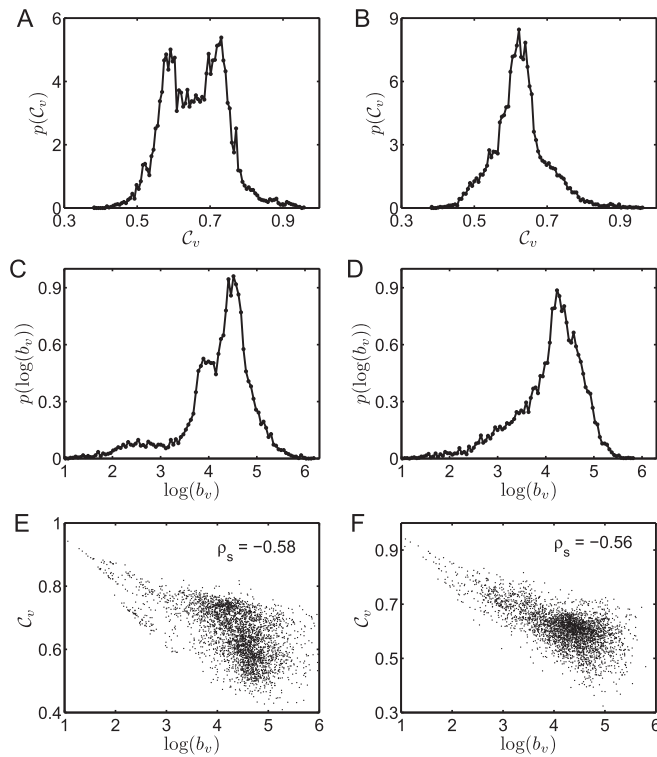


FIG. 7. Probability distribution functions of the local RN properties ((a) and (b)) C_v and ((c) and (d)) $\log b_v$ for the experimental data of electrochemical oscillations in the ((a) and (c)) low-temperature and ((b) and (d)) high-temperature regimes. Panels ((e) and (f)) display the associated scatter plots (C_v vs. $\log b_v$) as well as the values of the rank-order correlation coefficient ρ_s (Spearman's Rho) between both measures.

In contrast to the general qualitative spatial pattern, the empirical distributions of C_v and $\log b_v$ clearly differ qualitatively between high and low temperatures (Fig. 7). This result is consistent with the findings for the PSD and recurrence time distributions discussed in Sec. III C. From the geometric perspective, the attractor at low temperatures is more bundled in phase space, while the observed states fill a larger part of phase space more homogeneously (with a much stronger fragmentation) at higher temperatures (cf. Fig. 5(a)). Specifically, Figs. 2 and 3 show that the chaotic attractor at low temperatures has a clearly visible band structure. This fact is also manifested in the two distinct peaks in the probability density functions of C_v and b_v at low temperatures, which are missing at high temperatures (compare Figs. 7(a) and 7(c) with Figs. 7(b) and 7(d)).

In order to understand the bimodality of the distributions of C_v and $\log b_v$ at low temperatures, we note that since b_v is based on shortest paths on the network, the existence of relatively large gaps between the individual bands of the attractor (Fig. 2(a)) leads to two clusters of paths between vertices at low and high values of x that are characterized by different expected lengths. In turn, if these bands are sufficiently close (i.e., $\langle \mathcal{O}(\varepsilon) \rangle$, Fig. 2(b)), shortest paths can cross these gaps instead of taking “detours,”⁵⁸ resulting in a continuum of shortest path lengths without distinct preferred values. In a similar way, vertices on narrow “isolated” bands on the chaotic attractor are likely to have larger values of C_v due to

geometric reasons,^{58,64} which leads to the distinct secondary peak of $p(C_v)$ at $C_v > 0.7$ in the low-temperature regime (Fig. 7(a)) that is missing at higher temperatures (Fig. 7(b)). In this spirit, the observed bimodality for the considered experiments is closely related to the emergence of the chaotic attractor due to period-doubling bifurcations.⁷⁷ We note that this specific route to chaos actually gives rise to phase-coherent oscillations in the classical viewpoint based on the PSD.^{19–21} The distinct behavior of C_v and b_v additionally confirms our previous statement that both measures provide complementary aspects of the local fragmentations of the systems' attractor.⁶⁰ In fact, both characteristics display significant anti-correlations (Figs. 7(e) and 7(f)) that do not differ markedly between both cases.

Next, we study the behavior of selected statistics of the distributions of local network properties, such as standard deviation and skewness, in addition to the global network characteristics to obtain values characterizing structural differences in attractor geometry. From the quantitative point of view, we note that the different “degrees” of structural complexity can be well distinguished by all considered local as well as global RN measures (Table I). As the latter increases from low- to high-temperature case, the transitivity-based network measures decrease, which is consistent with the interpretation of local clustering coefficient as well as global network transitivity as measures for the effective (local and global) dimensionality of the system.⁶⁴ Thus, \mathcal{T} , \mathcal{C} , and σ_C show the behavior that is to be expected (i.e., lower values for more complex dynamics) as long as the network structure is not dominated by secondary geometric effects such as the presence of homoclinic points (as it is the case in, e.g., in the Rössler system²⁹). At the same time, the obtained values of the average path length consistently decrease, which is also consistent with previous results on the behavior of global recurrence network measures.⁶³

C. Changes in attractor geometry

As seen in Sec. III, the formerly reported enhanced phase diffusion at high temperatures mainly results from a gradual increase of dynamical complexity of the chaotic attractor and does not reflect qualitatively different structural

TABLE I. Mean values and standard deviations (in brackets) of different RN characteristics for the experimental cases I and II, obtained from 100 independent samples of $N = 10\,000$ state vectors randomly selected from the embedded time series. Note that all measures allow a discrimination between both cases with high confidence.

	I	II
\mathcal{C}	0.6653 (0.0015)	0.6227 (0.0011)
\mathcal{T}	0.6752 (0.0034)	0.6223 (0.0017)
\mathcal{L}	9.2418 (0.0691)	6.8445 (0.0397)
\mathcal{R}	0.8420 (0.0068)	0.8100 (0.0067)
σ_C	0.0842 (0.0010)	0.0745 (0.0009)
$\sigma_{\log b}$	0.7292 (0.0071)	0.6888 (0.0050)
γ_C	0.1095 (0.0399)	0.8415 (0.0396)
$\gamma_{\log b}$	-1.1864 (0.0302)	-1.0321 (0.0277)

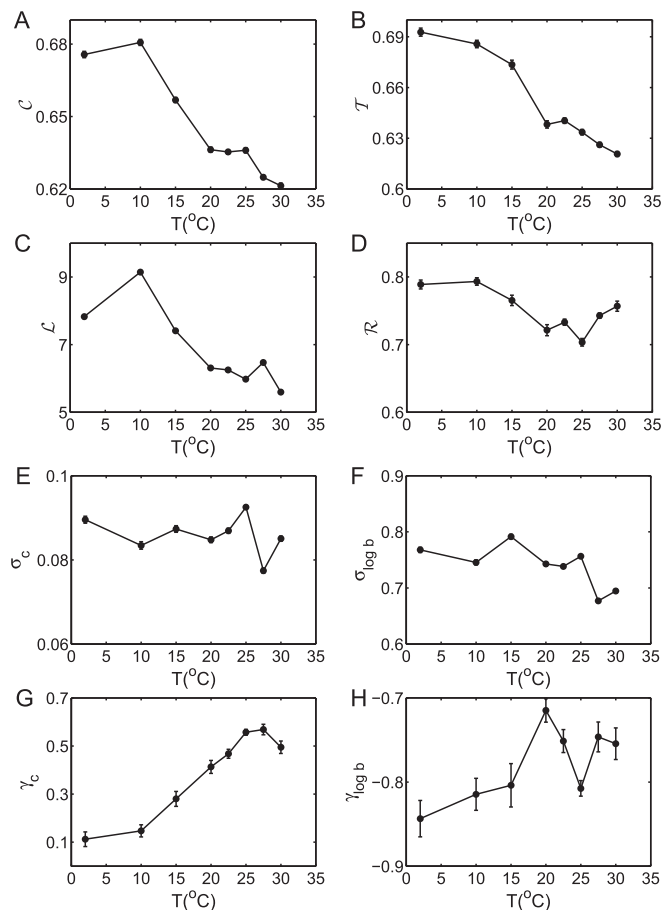


FIG. 8. Behavior of RN-based characteristics for the electrochemical oscillations in dependence on the temperature as the unique control parameter varied in the experimental campaign ($RR = 0.03$): (a) global clustering coefficient \mathcal{C} , (b) network transitivity \mathcal{T} , (c) average path length \mathcal{L} , (d) assortativity coefficient \mathcal{R} , ((e) and (f)) standard deviation, and ((g) and (h)) skewness of the local clustering coefficient and logarithmic betweenness centrality ($\sigma_{\mathcal{C}}$, $\sigma_{\log b}$, $\gamma_{\mathcal{C}}$, and $\gamma_{\log b}$, respectively). Error bars indicate the mean values and standard deviations from 100 independent realizations of the RN obtained from $N = 10\,000$ state vectors randomly selected from the whole embedded time series.

properties. Hence, although the electrochemical oscillations undergo a clear transition from low to higher complexity as the temperature increases, the structural phase coherence remains conserved. As Fig. 8 demonstrates, this is reflected by the structural attractor properties captured by RN analysis that do not change abruptly, but gradually with increasing temperature, which supports previous findings on the dynamical characteristics.¹⁵

Regarding the behavior of the different RN measures, we observe a consistent negative trend of \mathcal{C} and \mathcal{T} with increasing temperature. This observation can be interpreted as an increase in the number of degrees of freedom of the system or, to put it differently, its effective dimensionality.⁶⁴ Since such a higher dimensionality is typically reflected by an enhanced dynamical complexity, the corresponding results are consistent with those obtained when characterizing the system's nonlinear dynamics. Moreover, the decrease in \mathcal{L} is also a typical feature associated with a larger relative spread of the chaotic attractor in phase space (because of the emergence of geometric “shortcuts” in the RN between

distant points on the attractor⁵⁸), which is often observed (for conserved recurrence rate RR) as the dynamical complexity of the system increases.⁶³ With the exception of $\gamma_{\mathcal{C}}$ indicating a rising asymmetry of the distribution of local clustering coefficients of the RNs, the statistics associated with vertex properties of the RNs—as well as the assortativity \mathcal{R} —show a more ambiguous behavior that cannot be easily interpreted.

D. Mathematical model

In order to further support our findings for the experimental time series, we additionally apply RN analysis to simulated trajectories of a corresponding mathematical model introduced by Haim *et al.*⁷⁸ for describing the dynamics of anodic Ni dissolution processes. This model contains three relevant dynamical variables: the total surface coverage of NiOH + NiO, θ , the surface coverage of NiO, η , and the electrode potential, e . Considering a potentiostatic mode of cell operation, these variables are nonlinearly coupled and display a dynamics approximately described by the following ordinary differential equations (ODEs)

$$\begin{aligned} \frac{de}{dt} &= \frac{v - e}{r} - i_F(\theta, \eta) \\ \Gamma_1 \frac{d\theta}{dt} &= \frac{\exp(0.5e)}{1 + C_h \exp(e)} (1 - \theta) - bC_h \eta \exp(e) \\ \alpha \Gamma_2 \frac{d\eta}{dt} &= \exp(2e) (\theta - \eta) - cC_h \eta \exp(e) \end{aligned} \quad (11)$$

with the Faradic current

$$i_F = \left(\frac{C_h \exp(0.5e)}{1 + C_h \exp(e)} + a \exp(e) \right) (1 - \theta), \quad (12)$$

which we will use as our “macroscopic observable” in the following. $v = 60.8$ is the dimensionless circuit potential, $r = 50$ is the dimensionless resistance, and $C_h = 1200$, $a = 0.3$, $b = 6 \times 10^{-5}$, $c = 0.001$, $\Gamma_1 = 0.01$, and $\Gamma_2 = 0.8$ are fixed parameters.¹⁵ The ODEs are solved numerically applying a fourth-order Runge-Kutta method with the fixed step size $h = 0.01$ and a sampling time $\delta t = 0.2$. Note that the model does not have full temperature dependency for all parameters, however, it does reproduce the experimentally observed temperature-dependent increase of complexity during the metal dissolution process (for further details, see Ref. 15).

For consistency with recent work,¹⁵ we restrict our attention to parameter values $\alpha \in [1.0, 1.344]$ for which the system is in a chaotic oscillatory state. Repeating our RN analysis with trajectories obtained from numerical simulations of the above model, we find that the results are widely consistent with those obtained from the experimental data (Fig. 9). In particular, all four global network characteristics (\mathcal{L} , \mathcal{T} , \mathcal{C} , and \mathcal{R}) clearly display a decreasing trend with an increasing value of the model parameter α , which corresponds to an increasing temperature in experiments. In contrast, standard deviation and skewness of the local clustering coefficient show an increase with rising α (the latter again being consistent with the experimental findings), whereas the skewness of the betweenness centrality distribution displays

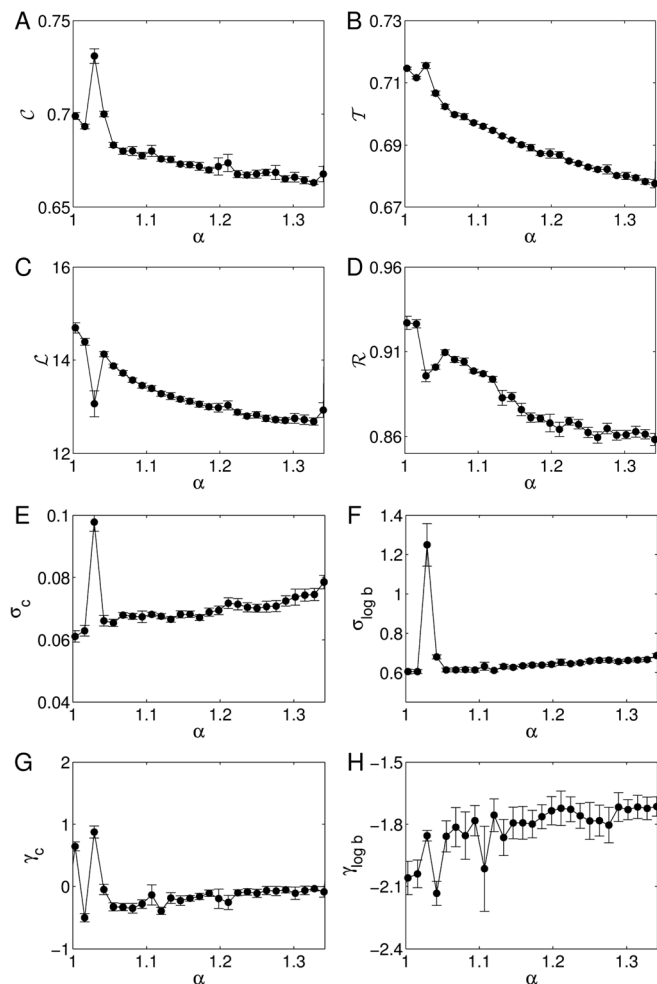


FIG. 9. As in Fig. 8 for realizations of the numerical model for Ni dissolution.⁷⁸

a more ambiguous behavior. This suggests that higher-order statistical characteristics of the distributions of local RN properties have a more limited power for characterizing changes in the underlying system's structural complexity, i.e., the results obtained for the experimental data are not a simple effect of different noise levels in individual measurements. In contrast, the corresponding mean values and standard deviations as well as the global RN properties provide consistent and interpretable results.

V. CONCLUSIONS

We have reconsidered the problem of distinguishing between phase coherent and non-phase-coherent chaotic oscillations from experimental records. In particular, we have compared various definitions of phase coherence and discussed in detail the use of an alternative geometric viewpoint for characterizing phase coherence, which appears more generally applicable under real-world conditions. Specifically, we have shown that the standard approach of computing the Hilbert phase directly from a measured signal can lead to pitfalls if the underlying chaotic attractor has a strongly asymmetric shape in phase space. The reason for this is that depending on the selected observable (or observation function) the attrac-

tor's (two-dimensional) projection in the reconstructed phase space can take very different shapes. In turn, within the framework of the Hilbert phase approach, a system is identified as phase-coherent if and only if its two-dimensional projection has the shape of a smeared limit cycle with rotations obeying a well-defined center at the origin of the considered coordinate system. The latter can crucially depend on the choice of the reference coordinate, a fact that has already been described in many dynamical systems such as the Lorenz and Rössler oscillators.

We have argued that the potentially severe dependence on the chosen projection is an intrinsic disadvantage of the classical Hilbert transform approach to phase coherence analysis. This problem can be solved by allowing for feasible (linear or nonlinear) coordinate transformations before applying the Hilbert transform. However, finding an appropriate transformation could be a challenging task on its own in case of systems with a very complex geometric shape of the attractor.

As a consequence, we suggest that phase coherence should be understood as a structural (rather than dynamic) feature, which could be characterized by measures explicitly describing the geometric shape of the system's attractor in its phase space without the necessity of any particular lower-dimensional projection. Among other approaches, recurrence network analysis provides a prospective framework for this purpose.²⁹ Specifically, it has been recently shown in Ref. 29 that there is a manifestation of true transitions between phase-coherent and noncoherent chaotic dynamics as observed in some well-studied complex systems (e.g., the Rössler and Mackey-Glass systems) in several characteristics of recurrence networks. However, at present it is not possible to use this knowledge for predicting a transition point between both regimes, or giving some critical values as potential discriminators between the two types of behavior. In contrast, we conjecture that such critical values are most likely system-dependent, since they reflect the specific structural organization of the chaotic attractor under study.

In general, we emphasize that in comparison with the use of dynamical characteristics, a purely geometric characterization of phase coherence has the additional advantage of being more robust in the presence of observational noise than traditional dynamics-based approaches. For example, noise can hide peaks in the power spectrum of a time series, whereas recurrence network analysis and related geometric methods can conserve the basic attractor properties such as a torus-like shape even in the presence of moderate noise levels.^{66,79} Hence, it can be challenging to decide about the presence of phase coherence using dynamical characteristics such as power spectral density, recurrence time distribution, or phase diffusion coefficient even after an appropriate coordinate transformation (see above) in case of noisy experimental data. These problems are partially avoided by considering the geometric viewpoint.

As a particular example, we have studied chaotic electrochemical oscillations based on experimental time series as well as a corresponding mathematical model. Our results demonstrated that the system's dynamics undergoes a gradual change towards more complex behavior as the temperature as

the fundamental control parameter of the system increases. However, the system remains (from a structural perspective) phase-coherent over the entire considered parameter range, even though the changes in many dynamical properties resemble observations traditionally attributed to noncoherent chaotic oscillations. In this respect, in the considered example the apparent absence of phase coherence reflected in the dynamical properties has been a projection effect that can be resolved by allowing for simple linear transformations of the reconstructed attractor. We propose that similar findings could also apply to other experimental data with an apparent absence of phase coherence.

Finally, we emphasize that our corresponding considerations are closely related to the problem of finding an optimal phase definition for a chaotic system.^{80–84} Achieving a better understanding of the linkage between both geometric and optimal phase approaches will be a subject of future research.

ACKNOWLEDGMENTS

This work has been partially funded by the Leibniz society (Project ECONS) and the Federal Ministry for Education and Research (BMBF) via the Potsdam Research Cluster for Georisk Analysis, Environmental Change and Sustainability (PROGRESS). Y.Z. has been supported by the National Natural Science Foundation of China (Grant No. 11135001) and a Hong Kong Polytechnic University Postdoctoral Fellowship. I.Z.K. and M.W. acknowledge support by the National Science Foundation under Grant No. CHE-0955555.

- ¹*Chaotic Oscillators—Theory and Applications*, edited by T. Kapitaniak (World Scientific, Singapore, 1992).
- ²P. S. Landa, *Regular and Chaotic Oscillations* (Springer, Berlin, 2001).
- ³A. Nayfeh and D. Mook, *Nonlinear Oscillations* (Wiley, New York, 1979).
- ⁴J. Guckenheimer and P. Holmes, *Nonlinear Oscillations, Dynamical Systems, and Bifurcations of Vector Fields*, 3rd ed. (Springer, New York, 1990).
- ⁵A. Lichtenberg and M. Leiberman, *Regular and Chaotic Dynamics*, 2nd ed. (Springer, Berlin, 1992).
- ⁶H. Kantz and T. Schreiber, *Nonlinear Time Series Analysis*, 2nd ed. (Cambridge University Press, Cambridge, 2004).
- ⁷J. C. Sprott, *Chaos and Time-Series Analysis* (Oxford University Press, Oxford, 2003).
- ⁸M. G. Rosenblum, A. S. Pikovsky, and J. Kurths, *Phys. Rev. Lett.* **76**, 1804 (1996).
- ⁹A. Pikovsky, M. Rosenblum, and J. Kurths, *Synchronization—A Universal Concept in Nonlinear Sciences* (Cambridge University Press, 2001).
- ¹⁰J. Y. Chen, K. W. Wong, and J. W. Shuai, *Phys. Lett. A* **285**, 312 (2001).
- ¹¹G. V. Osipov, B. Hu, C. Zhou, M. V. Ivanchenko, and J. Kurths, *Phys. Rev. Lett.* **91**, 024101 (2003).
- ¹²I. Z. Kiss, Q. Lv, and J. L. Hudson, *Phys. Rev. E* **71**, 035201 (2005).
- ¹³M. C. Romano, M. Thiel, J. Kurths, I. Z. Kiss, and J. Hudson, *Europhys. Lett.* **71**, 466 (2005).
- ¹⁴C. Letellier and L. A. Aguirre, *Chaos* **12**, 549 (2002).
- ¹⁵M. Wickramasinghe and I. Z. Kiss, *Chaos* **20**, 023125 (2010).
- ¹⁶D. Farmer, J. Crutchfield, H. Froehling, N. Packard, and R. Shaw, *Ann. New York Acad. Sci.* **357**, 453 (1980).
- ¹⁷Y. Oono and M. Osikawa, *Prog. Theor. Phys.* **64**, 54 (1980).
- ¹⁸K. Ito, Y. Oono, H. Yamazaki, and K. Hirakawa, *J. Phys. Soc. Jpn.* **49**, 43 (1980).
- ¹⁹E. N. Lorenz, *Ann. New York Acad. Sci.* **357**, 282 (1980).
- ²⁰J. D. Farmer, *Phys. Rev. Lett.* **47**, 179 (1981).
- ²¹J. D. Farmer, *Physica D* **4**, 366 (1982).
- ²²I. Schreiber and M. Marek, *Phys. Lett. A* **91**, 263 (1982).

- ²³E. F. Stone, *Phys. Lett. A* **163**, 367 (1992).
- ²⁴J. B. Gao, *Phys. Rev. E* **63**, 066202 (2001).
- ²⁵G. Powell and I. Percival, *J. Phys. A* **12**, 2053 (1979).
- ²⁶J. Crutchfield, D. Farmer, N. Packard, R. Shaw, G. Jones, and R. Donnelly, *Phys. Lett. A* **76**, 1 (1980).
- ²⁷S. Blacher and J. Perdag, *Physica D* **3**, 512 (1981).
- ²⁸A. Ruzmaikin, J. Feynman, and V. Kosacheva, *The Solar Cycle*, Astronomical Society of the Pacific Conference Series Vol. 27, edited by K. L. Harvey (ASP, San Francisco, 1992), pp. 547–556.
- ²⁹Y. Zou, R. V. Donner, and J. Kurths, *Chaos* **22**, 013115 (2012).
- ³⁰R. Donner, in *Nonlinear Time Series Analysis in the Geosciences: Applications in Climatology, Geodynamics and Solar-Terrestrial Physics*, edited by R. V. Donner and S. M. Barbosa (Springer, Berlin, 2008), pp. 355–385.
- ³¹O. E. Rössler, *Phys. Lett. A* **57**, 397 (1976).
- ³²M. Thiel, M. Romano, J. Kurths, M. Rolf, and R. Kliegl, *Europhys. Lett.* **75**, 535 (2006).
- ³³S. Boccaletti, E. Allaria, and R. Meucci, *Phys. Rev. E* **69**, 066211 (2004).
- ³⁴H. Fujisaka, T. Yamada, G. Kinoshita, and T. Kono, *Physica D* **205**, 41 (2005).
- ³⁵A. S. Zakharaova, T. E. Vadivasova, and V. S. Anishchenko, *Int. J. Bifurcation Chaos* **18**, 2877 (2008).
- ³⁶A. S. Pikovsky and J. Kurths, *Phys. Rev. Lett.* **78**, 775 (1997).
- ³⁷C. S. Zhou, J. Kurths, E. Allaria, S. Boccaletti, R. Meucci, and F. T. Arecchi, *Phys. Rev. E* **67**, 066220 (2003).
- ³⁸N. H. Packard, J. P. Crutchfield, J. D. Farmer, and R. S. Shaw, *Phys. Rev. Lett.* **45**, 712 (1980).
- ³⁹F. Takens, in *Dynamical Systems and Turbulence, Warwick 1980*, Lecture Notes in Mathematics Vol. 898, edited by D. Rand and L.-S. Young (Springer, New York, 1981), pp. 366–381.
- ⁴⁰E. Lorenz, *J. Atmos. Sci.* **20**, 130 (1963).
- ⁴¹R. Miranda and E. Stone, *Phys. Lett. A* **178**, 105 (1993).
- ⁴²C. Letellier and R. Gilmore, *Phys. Rev. E* **63**, 016206 (2000).
- ⁴³M. Thiel, M. Romano, and J. Kurths, *Phys. Lett. A* **330**, 343 (2004).
- ⁴⁴G. Robinson and M. Thiel, *Chaos* **19**, 023104 (2009).
- ⁴⁵J.-P. Eckmann, S. O. Kamphorst, and D. Ruelle, *Europhys. Lett.* **4**, 973 (1987).
- ⁴⁶N. Marwan, M. Romano, M. Thiel, and J. Kurths, *Phys. Rep.* **438**, 237 (2007).
- ⁴⁷M. Thiel, M. Romano, P. Read, and J. Kurths, *Chaos* **14**, 234 (2004).
- ⁴⁸N. Asghari, C. Broeg, L. Carone, R. Casas-Miranda, J. C. C. Palacios, I. Csillik, R. Dvorak, F. Freistetter, G. Hadjivantsides, H. Hussmann *et al.*, *Astron. Astrophys.* **426**, 353 (2004).
- ⁴⁹W. von Bloh, M. C. Romano, and M. Thiel, *Nonlin. Processes Geophys.* **12**, 471 (2005).
- ⁵⁰J. Zbilut and C. Webber, *Phys. Lett. A* **171**, 199 (1992).
- ⁵¹C. Webber and J. Zbilut, *J. Appl. Physiol.* **76**, 965 (1994).
- ⁵²L. Trulla, A. Giuliani, J. Zbilut, and C. Webber, *Phys. Lett. A* **223**, 255 (1996).
- ⁵³N. Marwan, N. Wessel, U. Meyerfeldt, A. Schirdewan, and J. Kurths, *Phys. Rev. E* **66**, 026702 (2002).
- ⁵⁴J. B. Gao, *Phys. Rev. Lett.* **83**, 3178 (1999).
- ⁵⁵J. B. Gao, Y. H. Cao, L. Y. Gu, J. G. Harris, and J. C. Principe, *Phys. Lett. A* **317**, 64 (2003).
- ⁵⁶M. Thiel, M. Romano, and J. Kurths, *Izv. VUZov Appl. Nonlin. Dyn.* **11**, 20 (2003), e-print arXiv:nlin/0301027v1.
- ⁵⁷N. Marwan, J. F. Donges, Y. Zou, R. V. Donner, and J. Kurths, *Phys. Lett. A* **373**, 4246 (2009).
- ⁵⁸R. V. Donner, Y. Zou, J. F. Donges, N. Marwan, and J. Kurths, *New J. Phys.* **12**, 033025 (2010).
- ⁵⁹Z. Gao and N. Jin, *Phys. Rev. E* **79**, 066303 (2009).
- ⁶⁰R. V. Donner, Y. Zou, J. F. Donges, N. Marwan, and J. Kurths, *Phys. Rev. E* **81**, 015101 (2010).
- ⁶¹R. V. Donner, M. Small, J. F. Donges, N. Marwan, Y. Zou, R. Xiang, and J. Kurths, *Int. J. Bifurcation Chaos* **21**, 1019 (2011).
- ⁶²R. V. Donner, J. F. Donges, Y. Zou, N. Marwan, and J. Kurths, *Proc. NOLTA* **2010**, 87–90.
- ⁶³Y. Zou, R. V. Donner, J. F. Donges, N. Marwan, and J. Kurths, *Chaos* **20**, 043130 (2010).
- ⁶⁴R. V. Donner, J. Heitzig, J. F. Donges, Y. Zou, N. Marwan, and J. Kurths, *Europhys. J. B* **84**, 653 (2011).
- ⁶⁵J. F. Donges, J. Heitzig, R. V. Donner, and J. Kurths, *Phys. Rev. E* **85**, 046105 (2012).
- ⁶⁶F. Strozzi, K. Poljansek, F. Bono, E. Gutiérrez, and J. M. Zaldívar, *Int. J. Bifurcation Chaos* **21**, 1047 (2011).

- ⁶⁷Y. Zou, J. Heitzig, R. V. Donner, J. F. Donges, J. D. Farmer, R. Meucci, S. Euzzor, N. Marwan, and J. Kurths, *Europhys. Lett.* **98**, 48001 (2012).
- ⁶⁸A. Facchini and H. Kantz, *Phys. Rev. E* **75**, 036215 (2007).
- ⁶⁹M. Newman, *SIAM Rev.* **45**, 167 (2003).
- ⁷⁰S. Boccaletti, V. Latora, Y. Moreno, M. Chavez, and D. U. Hwang, *Phys. Rep.* **424**, 175 (2006).
- ⁷¹L. D. F. Costa, F. A. Rodrigues, G. Travieso, and P. R. V. Boas, *Adv. Phys.* **56**, 167 (2007).
- ⁷²L. C. Freeman, *Soc. Networks* **1**, 215 (1979).
- ⁷³D. J. Watts and S. H. Strogatz, *Nature* **393**, 440 (1998).
- ⁷⁴A. Barrat and M. Weigt, *Eur. Phys. J. B* **13**, 547 (2000).
- ⁷⁵M. E. J. Newman, *Phys. Rev. E* **64**, 016131 (2001).
- ⁷⁶M. E. J. Newman, *Phys. Rev. Lett.* **89**, 208701 (2002).
- ⁷⁷J. Davidsen, I. Z. Kiss, J. L. Hudson, and R. Kapral, *Phys. Rev. E* **68**, 026217 (2003).
- ⁷⁸D. Haim, O. Lev, L. M. Pismen, and M. Sheintuch, *J. Phys. Chem.* **96**, 2676 (1992).
- ⁷⁹R. Xiang, J. Zhang, X.-K. Xu, and M. Small, *Chaos* **22**, 013107 (2012).
- ⁸⁰B. Kralemann, L. Cimponeriu, M. Rosenblum, A. Pikovsky, and R. Mrowka, *Phys. Rev. E* **76**, 055201 (2007).
- ⁸¹B. Kralemann, L. Cimponeriu, M. Rosenblum, A. Pikovsky, and R. Mrowka, *Phys. Rev. E* **77**, 066205 (2008).
- ⁸²J. T. C. Schwabedal and A. Pikovsky, *Phys. Rev. E* **81**, 046218 (2010).
- ⁸³J. T. C. Schwabedal and A. Pikovsky, *Eur. Phys. J. Spec. Top.* **187**, 63 (2010).
- ⁸⁴J. T. C. Schwabedal, A. Pikovsky, B. Kralemann, and M. Rosenblum, *Phys. Rev. E* **85**, 026216 (2012).